VRIJE
UNIVERSITEIT
BRUSSEL

Graduation thesis submitted in partial fulfilment of blah

SOMETHING ABOUT HIGGS+CHARM

my thesis subtitle

Felix Heyen

March 2026

Promotors: prof. dr. Michael Tytgat prof. dr. Gerrit Van Onsem

sciences and bioengineering sciences

Abstract

My abstract

Contents

Chapter 1

Introduction

The Standard Model (SM) of particle physics is the theory that best decribes our current understanding of fundamental particles and their interactions. It describes a broad range of phenomena and makes a plethora predictions for these, many of which have been confirmed via measurement to great degrees of accuracy [1]. A noteable feature of the SM is the Brout-Englert-Higgs (BEH) mechanism [2][3], which predicts the existance of a Brout-Englert-Higgs (or often simply Higgs) boson. The EBH mechanism is considered a central part of the SM as it provides a unique mechanism by which SM particles may acquire mass through their interaction with the Higgs boson. As such, the experimental discovery of a Higgs-like scalar boson in 2012 [4][5] was a major milestone in particle physics. Since this discovery, a significant open question in particle physics has been whether this particle indeed behaves entirely in an SM-like way. Measuring the exact properties of the discovered scalar particle has thus been a major feature of LHC experiments such as the CMS collaboration [6]. A significant subset of these properties are the so-called Yukawa interactions between the Higgs boson and massive fermions. As can be seen in Figure 1.1, a number of these have previously been measured and indeed align with the values expected from the SM. However, the measurement of the Yukawa couplings of several of the lighter fermions still remain an open challenge as these couplings decrease in strength with smaller fermion masses.

The next lightest fermion candidate for such a measurement is the charm quark. Consequentially, the study of the Yukawa-coupling between the Higgs boson and the charm quark is of significant interest [7]. Apart from a brief discussion of the SM, this section introduces the charm-Yukawa coupling. Additionally, LHC processes may be targeted to exploit their sensitivity to the Higgs-charm Yukawa coupling with an experiment such as the CMS detector are discussed.

1.1 The Standard Model of particle physics

The SM is formulated as through the formalism of Quantum Field Theory (QFT) [**something here**]. This is a formalism that combines concepts of classical field theory, quantum machanics as well as special relativity into a single, coherent description of fundamental particles as excitations of underlying fields that pervade space-time. In this description, SM particles fall into two categories: fermions and bosons. The former are the massive particles which may make up the matter of the universe while the latter are the force-carrying particles of the strong and electro-weak forces. The distinction between these categories is made based on the spin of the particle, which may be of either half-integer or integer respectively.

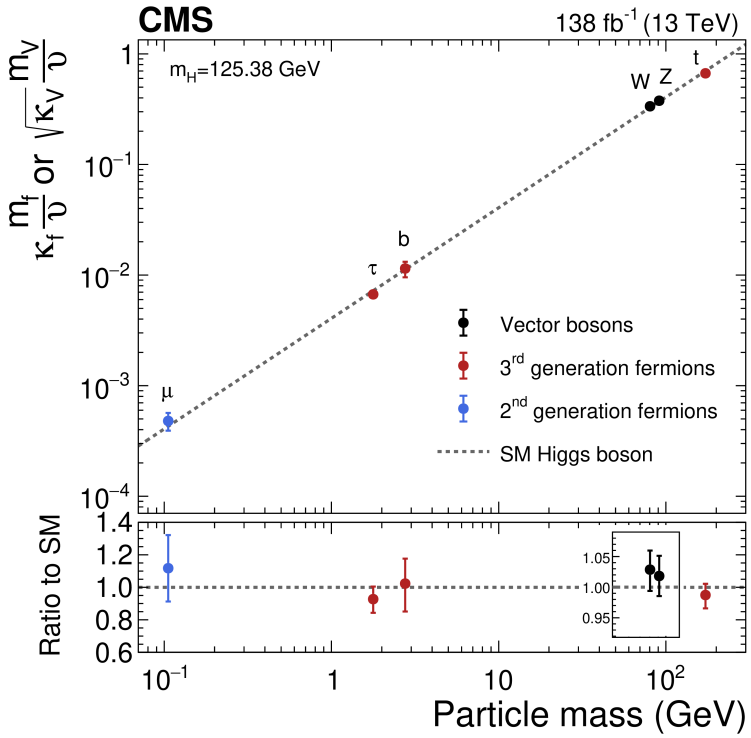

Figure 1.1: The measured coupling modifiers κ_f and κ_V of the coupling between the Higgs boson and fermions as well as heavy gauge bosons as functions of fermion or gauge boson mass m_f and m_V, where ν is the vacuum expectation value of the Higgs field. [6]

The fermion content of the SM consists of 12 unique particles. These include six leptons, namely the electron, muon and tau as well as their respective neutrinos as well as six different quarks that are distinguished by their so-called flavour. The different quark flavours include up, down, charm, strange, bottom and top and specifies a quark's mass eigenstate as well as electric charge. These fermions are typically arranged into three generations typically depicted as

$$\begin{pmatrix} e \\ \nu_e \end{pmatrix} \begin{pmatrix} \mu \\ \nu_\mu \end{pmatrix} \begin{pmatrix} \tau \\ \nu_\tau \end{pmatrix}, \begin{pmatrix} u \\ d \end{pmatrix} \begin{pmatrix} c \\ s \end{pmatrix} \begin{pmatrix} t \\ b \end{pmatrix}. \tag{1.1}$$

However, there are distinct differences between the leptons and quarks. Leptons carry integer (or no) charge while quarks carry fractional charges. More importantly, while both quarks and leptons may interact via the electro-weak force, only the quarks interact via the strong force. Due to the nature of the strong force, quarks almost exlusively form compositive states called hadrons. Lastly, the existence of anti-fermions must be mentioned. These carry the exact opposite quantum numbers (.e.g charge) as their fermion counterparts, though otherwise behave similarly (take the electron and positron for instance). For simplicity, references to a fermion in this work may be understood as referencing both the fermion and anti-fermion counterpart, unless otherwise explicitly indicated. Examples of the latter are e.g. referring explicitly to electrons e^- and positrons e^+ or charm quark c and anti-charm quark $\bar{c}$ pairs.

There exist 13 unique bosons in the SM. These include the photon γ, $W^\pm$ and Z which mediate the electro-weak force as well as 8 gluons g that mediate the strong force. The final piece is the Higgs boson. Contrary to the force carriers, which all are spin 1, the Higgs boson is spin 0. By interacting with the Higgs boson, the massive particles of the SM acquire their mass and is thus a central element of the SM.

Considering the introduced particles and forces, the SM has a rich and detailed phenomeology. A great example of a mathematically rigurous delineation of this can be found for example in [8]. Given the focus of this work on the Yukawa coupling between the Higgs boson and charm quark, only this aspect of the SM is discussed in further detail.

1.2 The Higgs-charm Yukawa coupling

The coupling that defines the strength of the interaction between massive fermions and the Higgs boson is the so-called Yukawa coupling. To better understand this and associated concepts, some knowledge of the electro-weak sector of the SM is required. These are discussed in this section while a comprehensive overview may be found in [9].

To understand the origin of the Yukawa-couplings, a brief discussion of Lagrangian densities, gauge transformations and the role of symmetries in the SM is warranted. The Lagrangian density $\mathcal{L}(\phi_i; a_i)$ is a quantity dependent on a set of fields ϕ_i and constants a_i from which the equations of motions for the particles associated with these fields may be derived. Commonly, theories of particles and their behaviour in a QFT are thus defined through the formulation of a Lagrangian density. The form of this expression determines the nature of the particles that are included as well as their interactions. A central component to the way in which particle interactions are introduced in the SM is the concept of gauge symmetries. These originate from the fact that the quantum fields in a QFT carry phase information, which may depend on the space-time coordinate of the field. This phase information describes (local) degrees of freedom of

the field and should have no effect on the physical obersvables of the system. Thus, $\mathcal{L}$ should remain invariant under arbitary phase transformations. Such transformations are typically referred to as a choice of gauge and such an invariance is accordingly referred to as a *local gauge symmetry.*

In the Lagrangian of the SM, invariance in the presence of local gauge symmetries is insured through the addition of additional fields. These gauge fields couple to the previously existing fields and effectively serve as mediators of phase information between space-time points of the original fields. It is exactly these gauge fields which we identify as the fields force-mediating bosons introduced previously and which are required to maintain local gauge symmetry. A very interesting conclusion from this is that the dynamics of the bosons and the corresponding force are determined entirely by the structure of the local gauge symmetry that must be preserved. For the electro-weak force, the corresponding symmetry is referred to as $\mathbf{SU(2)}_{\mathrm{L}}\,\mathrm{x}\,\mathbf{U(1)}_{Y}$. Here, the L denotes that the associated force only acts on left-handed chiral particles while the Y denotes the charge that is carried by the corresponding bosons and is referred to as the weak hypercharge. There are a total of four boson associated with the electro-weak force. These are the photon γ that mediates the electromagnetic force as well as the electromagnetically charged $\mathrm{W}^{\pm}$ and electromagnetically neutral Z boson that mediate the weak force.

With these concepts in mind the nature of the electro-weak sector's Lagrangian in the SM may be discussed. Naively, the form of this would be given by

$$\mathcal{L}_{\mathrm{EW}} = i\overline{\psi}_L\gamma^\mu D_\mu^L\psi_L + i\overline{\psi}_R\gamma^\mu D_\mu^R\psi_R - \frac{1}{2}\mathrm{Tr}\left(W_{\mu\nu}^a W^{a\mu\nu}\right) - \frac{1}{4}B_{\mu\nu}B^{\mu\nu}\,. \tag{1.2}$$

for a generic combination of a left-handed isospin doublet ψ_L and and right-handed isospin singlet ψ_L. The individual elements of $\mathcal{L}_{\mathrm{EW}}$ are briefly summarised below

g' :	coupling constant of $\mathrm{U}(1)_Y$
g :	coupling constant of $\mathrm{SU}(2)_L$
ψ_L,	left-handed isospin doublet
ψ_R,	right-handed isospin doublet
B_μ :	gauge field of $\mathrm{U}(1)_Y$
W_μ^a :	gauge fields of $\mathrm{SU}(2)_L$, $a = 1, 2, 3$
$W_{\mu\nu}$:	field strength tensor
$B_{\mu\nu}$:	field strength tensor
$t^a = \frac{\sigma^a}{2}$,	$\mathrm{SU}(2)$ generators
$Y_L = -1$,	left chiral hypercharge
$Y_R = -2$,	right chiral hypercharge
$D_\mu^L = \partial_\mu + ig'\frac{Y_L}{2}B_\mu + igt^aW_\mu^a$	
$D_\mu^R = \partial_\mu + ig'\frac{Y_R}{2}B_\mu$	

The terms $D_\mu^{L/R}$ are so-called covariant derivates that ensure the local $\mathrm{SU(2)_L\,x\,U(1)}_Y$ gauge symmetry is uphheld for $\mathcal{L}_{EW}$. In this formulation, the observed charged gauge bosons $\mathrm{W}^\pm$ arise from linear combinations of the W_1 and W_2 gauge fields

$$W^\pm = \frac{1}{\sqrt{2}}(W_1 \mp iW_2), \tag{1.3}$$

while the Z boson and photon γ arise from linear combinations of the W_3 and B gauge fields achieved via a rotation

$$\begin{pmatrix}\gamma\\ Z\end{pmatrix} = \begin{pmatrix}\cos\theta_\mathrm{W} & \sin\theta_\mathrm{W}\\ -\sin\theta_\mathrm{W} & \cos\theta_\mathrm{W}\end{pmatrix}\begin{pmatrix}B\\ W_3\end{pmatrix}. \tag{1.4}$$

with the weak mixing angle θ_W.

The massive natures of of the $\mathrm{W}^\pm$ and Z bosons, as first reported in [10], are however incompatible with such a formulation. This is as naive mass term such as

$$m_W^2 W_\mu^+ W^{-,\mu} + \frac{1}{2}m_Z^2 Z_\mu Z^\mu. \tag{1.5}$$

do not remain invariant under arbitrary $\mathrm{SU(2)_L}$ gauge transformations. This is as gauge fields A_μ generically transform as

$$A_\mu \rightarrow A_\mu^{'} = A_\mu - \frac{1}{g}\partial_\mu \mathcal{V}(x) \tag{1.6}$$

where $\mathcal{V}(x)$ is some arbitrary phase. Substituting Equation 1.6 into Equation 1.5 thus introduces additional terms that do not cancel. The same is true for fermion mass terms in the form of

$$m_\mathrm{f}\overline{\psi}\psi. \tag{1.7}$$

There is however a subtle distinction in this case, as the invariance breaking terms in Equation 1.7 arise from the different transformation behaviour of the ψ_L and ψ_R components of ψ under $\mathrm{SU(2)_L\,x\,U(1)}_Y$ gauge transformations.

1.2.1 The Brout-Englert-Higgs mechanism

The BEH mechanism provides a way to circumvent the gauge symmetry breaking nature of the aforementioned generic mass terms. This is achieved through a porcess referred to as spontaneous symmetry breaking. A spontaneously broken symmetry refers to a symmetry that is upheld in a global view of the system (i.e. the overall Lagrangian density $\mathcal{L}_\mathrm{EW}$ remains invariant under a relevant gauge transformation) while the energetic ground state of the system explicitly breaks this symmetry. This is a process formally described by the Goldstone theorem [11]that states that each broken symmetry in a relativistic QFT generates an additional massless boson. These introduce additional degrees of freedom into the theory and are coined Goldstone bosons. The

BEH mechanism exploits this by adding an additional term

$$\mathcal{L}_{\text{Higgs}} = D_\mu \phi^\dagger D^\mu \phi - V(\phi) \tag{1.8}$$

$$V(\phi) = -\mu^2 \phi^\dagger \phi + \lambda (\phi^\dagger \phi)^2. \tag{1.9}$$

to $\mathcal{L}_{\text{EW}}$ with the complex field ϕ. This is a $\text{SU}(2)_L$ doublet

$$\phi = \begin{pmatrix} \phi^+ \\ \phi^0 \end{pmatrix} \tag{1.10}$$

with the scalar components ϕ^+ and ϕ^0. Here, $V(\phi)$ corresponds to the potential energy term of the feild. Again, the covariant derivative

$$D_\mu = \partial_\mu + ig' \frac{Y_\phi}{2} B_\mu + igt^a W_\mu^a \tag{1.11}$$

ensures $\mathcal{L}_{\text{Higgs}}$ remains locally gauge invariant under $\text{SU(2)}_\text{L} \,\text{x}\, \text{U(1)}_Y$ transformations. The constants of the potential term Equation 1.9 are chosen in such a way that the ground state of V is non-zero. This can be achieved by choosing them such that $\lambda > 0$ and $\mu^2 > 0$. The result is a ground state of V that is identified as the vacuum expectation

$$v = \sqrt{\frac{\mu^2}{2\lambda}}\,. \tag{1.12}$$

The center of the potential is now an unstable local maximum and the only stable configuration can be found in the non-zero ground state. Through this, the symmetry of the potential is effectively broken. A popular choice of gauge for ϕ is

$$\phi = \begin{pmatrix} 0 \\ v + \frac{h}{\sqrt{2}} \end{pmatrix} \tag{1.13}$$

where h is a new scalar field that is used to parametrise radial perturbations of the potential's ground state. This choice is referred to as the unitary gauge and h is identified as the field corresponding to the physical Higgs boson. By expanding Equation 1.8 with this choice of ϕ, a range of terms are introduced to $\mathcal{L}_{\text{EW}}$. These contain a variety of interaction terms between the gauge fields and the Higgs field, as well as newly generated mass terms for the Z and W bosons

$$\left(\frac{g}{2}\right)^2 v^2 W_\mu^+ W^{\mu-} = m_\text{W}^2 W_\mu^+ W^{\mu-} \tag{1.14}$$

$$\left(\frac{\sqrt{g^2+g'}}{2}\right)^2 v^2 Z_\mu Z^\mu = m_\text{Z}^2 Z_\mu Z^\mu\,. \tag{1.15}$$

This can be understood to mean that the electro-weak coupling constants g and g' along with v effectively determine the mass of the Z and $\text{W}^\pm$ bosons. A full description and compilation of all the terms of the electro-weak Lagrangian density of the SM can be found in **??**.

1.2.2 The Yukawa couplings

By including the Higgs contribution in our theory, mass terms for fermions may now be generated by including a term of the form

$$\mathcal{L}_{\text{Yukawa}} = -y_{\text{f}}\overline{\psi}\phi\psi, \tag{1.16}$$

$$= -y_{\text{f}}v\overline{\psi}\psi(1 + \frac{1}{v}\frac{h}{\sqrt{2}}) \tag{1.17}$$

which is invariant under $\text{SU(2)}_{\text{L}}\,\text{x}\,\text{U(1)}_{Y}$ gauge transformations due to the addition of ϕ. Similarly to the W and Z mass terms, the relation

$$m_{\text{f}} = y_{\text{f}}v. \tag{1.18}$$

is obtained. A curious feature of the SM is that the Yukawa-couplings y_{f} are free parameters of the theory with no a priori values. As a result these must be measured experimentally with the measurement of the charm quark Yukawa coupling y_{c} being the goal of this work. As the charm quark mass has previously been determined from experiment to be $m_{\text{c}} = 1.27$ GeV [1], a measurement of y_{c} thus represents an important consistency test of the SM. Another feature that can be read off from Equation 1.17 is that an interaction between fermions and the Higgs field is introduced with an interaction strength proportional to y_{c}. It is exactly this feature that may be exploited by experiments at the LHC to measure y_{c}.

1.3 Measuring the charm quark Yukawa coupling

By measuring the frequency of occurence of physics processes in which the coupling between the Higgs boson and charm quark appears, y_{c} may be determined. As such, a suitable process must be found that can be detected by an experiment such as CMS. These fall into two categories. The first consists of processes in which a Higgs boson decays into a charm and anti-charm quark pair ($\text{H}\rightarrow\text{c}\overline{\text{c}}$). Previous analysis of e.g. top quark pair and vector boson associated Higgs production has been able to observe a 95% CL upper limit on the charm quark Yukawa coupling modifier κ_{c} (see subsection 1.3.2 for a detailed discussion) of $\kappa_{\text{c}} < |3.5|$ [12], the most stringent limit to date. The second category consists of processes in which a Higgs boson is produced in association with a charm quark. This latter category of processes is the focus of this work and is henceforth referred to as the cH process.

1.3.1 The cH process

The cH process encompasses processes in proton-proton collisions in which a charm-quark is produced alongside a Higgs boson. At leading order, this consists of 2 processes sensitive to y_{c}, represented by the Feyman diagrams shown in Figure 1.2. The first two diagrams, namely the s and t-channel diagrams, constitute the y_{c}sensitive contribution. There exist also additional processes cH, mediated through the effective Higgs boson to gluon coupling, which are not sensitive to y_{c}. These account for approximately 80% of the inclusive cH cross section and thus represents a significant background to the cH process sensitive to the charm quark Yukawa coupling.

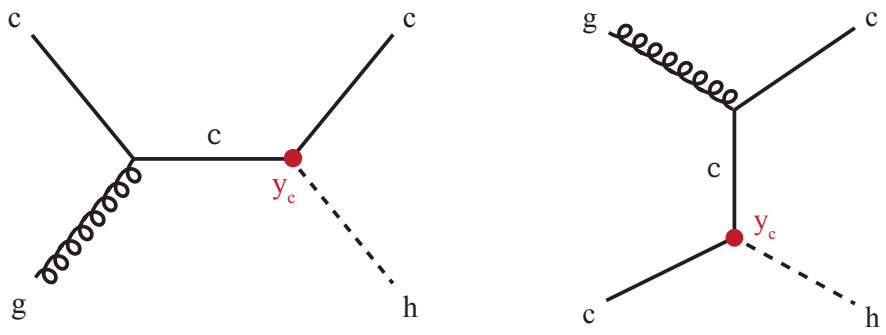

Figure 1.2: The leading order cH processes through which y_c may be probed. The red dot represents the coupling between the charm quark and Higgs boson and thus the sensitivity to y_c. The corresponding diagrams with an anti-charm quark $\bar{c}$ are implied.

Targeting the cH process to measure y_c is a relatively novel strategy in comparison to analyses that target H→c$\bar{c}$. A key advantage of this approach is that contributions from the abudant QCD background at the LHC are greatly reduced due to only needing to identify the flavour of single jet resulting from a charm quark, as opposed to two. Additionally, since the sensivity to y_c does not originate from the decay of the Higgs boson, the Higgs boson decay mode to target can be chosen freely. Especially signatures such as H→ZZ→4μ, which may be resolved cleanly by an experiment such as CMS, can be targeted. However, targeting the cH process also comes with drawbacks. A significant experimental difficulty results from the fact that the associated charm flavour jet are typically produced at very low transverse momenta p_T, as seen in **??**. These can be experimentally difficult to reconstruct and thus a significant portion of this signal may be lost due to detector acceptance effects. Another drawback is that Higgs boson decay channels such as H→ZZ→4μ have very small branching ratios (e.g. BR(H→ZZ→4μ) = 0.3% [1]) and thus the overall cross section of the cH process may be very small. As a result of these effects, a key challenge of a search for the cH process is expected to lie in its statistical uncertainty.

The cH process is of recent interest and results in the cH(WW) and cH($\gamma\gamma$) channels using Run 2 data of the CMS experiment are published. Upper limits on κ_c at 95% CL are reported with $|\kappa_c{}^{cH(WW)}| < 47$ [13] and $|\kappa_c{}^{cH(\gamma\gamma)}| < 38.1$ [14]. While not as sensitive as the limit observed in the H→c$\bar{c}$ channels, these nonetheless provide important complementary results and can contribute significantly in combination. This is especially important given that even at the High-Luminosity LHC, the projected sensitivity on the charm quark Yukawa coupling in individual channels is only starting to approach one [15].

1.3.2 The κ-framework

The κ-framework [16] is a tool to parametrise modifications to couplings between the Higgs boson and other particles with respect to the expected SM values of the couplings. For example, the coupling modifiers for the charm quark Yukawa coupling is introduced as

$$\kappa_f = \frac{y_f}{y_f^{SM}}. \tag{1.19}$$

where y_{f} is the measured Yukawa-coupling and $y_{\mathrm{f}}^{\mathrm{SM}}$ is the expected Yukawa-coulpling of the SM, calculated from the known charm quark mass. Thus modifications to the Yukawa-coupling of the charm quark are parametrised in this way as deviations from $\kappa_{\mathrm{c}} = 1$. However, y_{c} is not a quantity that can be measured directly. Instead a signal strength measurement μ_{if}, where i represents the production process and f represents the decay process, relative to the SM expectation is made. Thus a measurement of μ_{if} must be converted into an interpretation of κ_{c}. This is a step that contains some finer subtleties.

The rate of a Higgs production and decay process in relation to the expected SM signal (i.e. a signal strength) may be written as

$$\mu_{if} = \frac{\sigma_i \cdot \mathrm{BR}_f}{(\sigma_i \cdot \mathrm{BR}_f)^{\mathrm{SM}}}, \tag{1.20}$$

where σ_i is the production cross section in a given channel i and BR_f is the decay branching ratio in a given channel f. This can be rewritten as

$$\sigma_i \cdot \mathrm{BR}_f = \kappa_{r,i}\sigma_i^{\mathrm{SM}} \cdot \frac{\kappa_f \Gamma_f^{\mathrm{SM}}}{\Gamma_{\mathrm{H}}} \tag{1.21}$$

to give a general expression in which modifications to the production cross section and partial SM decay width Γ_f^{SF} are introduced via $\kappa_{r,i}$ and κ_f respectively. The denominator Γ_{H} represesents the total decay width which can be written as

$$\begin{aligned}\Gamma_{\mathrm{H}} =& \Gamma_{\mathrm{H}}^{\mathrm{SM}}(\kappa_{\mathrm{b}}^2 \mathrm{BR}_{\mathrm{bb}}^{\mathrm{SM}} + \kappa_{\mathrm{W}}^2 \mathrm{BR}_{\mathrm{WW}}^{\mathrm{SM}} + \kappa_{\mathrm{g}}^2 \mathrm{BR}_{\mathrm{gg}}^{\mathrm{SM}} + \kappa_{\tau}^2 \mathrm{BR}_{\tau\tau}^{\mathrm{SM}} + \kappa_{\mathrm{Z}}^2 \mathrm{BR}_{\mathrm{ZZ}}^{\mathrm{SM}} + \kappa_{\mathrm{c}}^2 \mathrm{BR}_{\mathrm{cc}}^{\mathrm{SM}} \\ &+ \kappa_{\gamma}^2 \mathrm{BR}_{\gamma\gamma}^{\mathrm{SM}} + \kappa_{\mathrm{Z}\gamma}^2 \mathrm{BR}_{\mathrm{Z}\gamma}^{\mathrm{SM}} + \kappa_{\mathrm{s}}^2 \mathrm{BR}_{\mathrm{ss}}^{\mathrm{SM}} + \kappa_{\mu}^2 \mathrm{BR}_{\mu\mu}^{\mathrm{SM}}) \qquad (1.22) \\ :=& \Gamma_{\mathrm{H}}^{\mathrm{SM}} \kappa_{\mathrm{H}}^2 \qquad (1.23)\end{aligned}$$

Here, $\Gamma_{\mathrm{H}}^{\mathrm{SM}}$ is the SM total decay width of the Higgs boson and $\mathrm{BR}_f^{\mathrm{SM}}$ are the branching ratios of the possible decay modes (the loop induced coupling of the Higgs boson to gluons and photons are included as independent quantities) where κ_f parametrises modifications thereof. Substituting Equation 1.23 into Equation 1.20, the rate modifier may be written as

$$\mu_{if} = \frac{\kappa_{r,i}^2 \kappa_f^2}{\kappa_{\mathrm{H}}^2}. \tag{1.24}$$

Now, assuming in the production of the Higgs boson only modifications to the charm quark Yukawa coupling plays a role as well as that the decay mode (e.g. $\mathrm{H} \to \mathrm{ZZ} \to 4\mu$) is unmodified, Equation 1.24 becomes

$$\mu_{if} = \frac{\kappa_{\mathrm{c}}^2}{\kappa_{\mathrm{H}}^2} \tag{1.25}$$

Using the flat direction approach discussed in [7] and [17], a simplification of κ_{H} can be introduced. This approach is based on the finding that, when performing fits to existing Higgs boson production and decay rates, increases in the Yukawa couplings of light quarks (including the charm quark) can be compensated by increases in the couplings of the gauge bosons and heavy fermions. This is referred to as a "flat direction" in the fit, where observed Higgs boson production and decay rates can be modeled equally well for any value of κ_{c} by a respective scaling of all

other processes. The authors thus replace the individual modifiers in the sum of Equation 1.22 with a single modifier κ. This allows Equation 1.24 to be rewritten as

$$\mu_{if} = \frac{\kappa^4}{\kappa^2(1-\mathrm{BR}_{\mathrm{cc}}^{\mathrm{SM}}) + \kappa_{\mathrm{c}}^2 \mathrm{BR}_{\mathrm{cc}}^{\mathrm{SM}}} \tag{1.26}$$

which has a solution for κ given by

$$\kappa = \frac{(1-\mathrm{BR}_{\mathrm{cc}}^{\mathrm{SM}})\mu}{2} + \frac{\sqrt{(1-\mathrm{BR}_{\mathrm{cc}}^{\mathrm{SM}})^2\mu^2 + 4\mu\mathrm{BR}_{\mathrm{cc}}^{\mathrm{SM}}\kappa_{\mathrm{c}}^2}.}{2}. \tag{1.27}$$

Here, the expected SM decay width $\mathrm{BR}_{\mathrm{cc}}^{\mathrm{SM}} = 0.3$ can be subsituted. Additionally, the fact that observed Higgs boson rates have been well measured to be close to their expected values (see e.g. [18]) can be reflected by setting $\mu \approx 1$, so that only a dependence on κ_{c} remains in the expression. Thus by replacing κ_{H} in Equation 1.25 with Equation 1.27, a final expression relating a measured signal strength of the cH process to κ_{c} is obtained, given by

$$\mu_{\sigma_{\mathrm{cH}}\mathrm{BR}(\mathrm{H}\to\mathrm{ZZ})} = \frac{2\kappa_{\mathrm{c}}^2}{0.97 + \sqrt{(0.97)^2 + 4\cdot 0.97\kappa_{\mathrm{c}}^2}}. \tag{1.28}$$

Rearranging for κ_{c} gives

$$\kappa_{\mathrm{c}} = \pm\frac{\sqrt{4\cdot 0.97\cdot \mu_{\sigma_{\mathrm{cH}}\mathrm{BR}(\mathrm{H}\to\mathrm{ZZ})}\cdot(1+\mu_{\sigma_{\mathrm{cH}}\mathrm{BR}(\mathrm{H}\to\mathrm{ZZ})})}}{2}. \tag{1.29}$$

Effectively, this approach in interpreting κ_{c} from a signal strength measurement $\mu_{\sigma_{\mathrm{cH}}\mathrm{BR}(\mathrm{H}\to\mathrm{ZZ})}$ thus ensures compatibility with existing Higgs boson rate measurements, given a non-unity value of κ_{c} leads to modifications of the Higgs boson partial decay widths. It should be noted that this already indirectly implies bounds on κ_{c}, as discussed in [7].

1.4 An EFT interpretation of the cH process

The cH process may also be interpreted in terms of Standard Model Effective Field Theory (SMEFT). In SMEFT theory, potential effects from physics processes not described by the SM (commonly referred to as beyond-the-SM or BSM physics) are parametrised in a mostly model-independent way. Specifically, the SMEFT framework can be used at colliders with a characteristic energy scale E to describe the effects of processes with a characteristic energy scale above E. This concept is illustrated in **??**.

Formally, SMEFT is a collection of all allowed interaction terms between fields that obey the rules of the SM. Most importantly, this means that said terms satisfy the gauge invariance conditions of the SM. Generically, this can be expressed as an expansion in the energy scale of the new physics scale Λ

$$\mathcal{L}_{\mathrm{SMEFT}} = \mathcal{L}_{\mathrm{SM}} + \sum_{d>4}\sum_{i}\frac{C_i}{\Lambda^{d-4}}\hat{O}_i^d \tag{1.30}$$

where $\mathcal{L}_{\text{SM}}$ is the SM lagrangian, O_i denotes a particular operator with a dimensionless coupling coefficient C_i and d denotes the dimension of the operator. This latter property arises from a dimensional analysis of a lagrangian and its fields, where energy dimensions of terms may be deduced from the requirement that the action

$$\text{S} = \int \mathcal{L} d^4x \tag{1.31}$$

remains dimensionless. As a result, $\mathcal{L}_{\text{SM}}$ is of energy dimension four. Since Λ carries an energy dimension of one, terms in the sum of Equation 1.30 scaled with $1/\Lambda^{d-4}$ must be compensated with an appropriate dimension of the operator O_i^d to ensure the overall terms also remain of energy dimension four. Consequently, operators in SMEFT are grouped by their energy dimension. In d=5, only one operator possible operator exists that violates lepton number [**d5Operator**] and is not relevant in this work. In d=6 however, a plethora of valid operators exist. In total, these amount to 59 different dimension six operators (modulo all possible flavour combinations), commonly represented in the Warsaw basis [**WarsawBasis**]. Since d=7 operators again violate lepton number and each additional dimension adds a suppresive factor of Λ^{-1}, a simplified SMEFT schema is commonly used in which only the contribution of d=6 operators is considered in the expansion. Thus Equation 1.30 simplifies to

$$\mathcal{L}_{\text{SMEFT}} = \mathcal{L}_{\text{SM}} + \sum_i \frac{C_i}{\Lambda^2} \hat{O}_i^{(6)} + \text{hc} \tag{1.32}$$

A good overview of SMEFT can be found in [**SMEFTOverview**].

1.4.1 The chromomagnetic dipole operator

A particular operator relevant to this work is referred to as the chromomagnetic dipole (CMD) operator $\hat{O}_{qG}$. For the charm quark, the CMD operator is written as

$$\hat{O}_{cG} = (\overline{q}_{2,L} \sigma^{\mu\nu} T^a c) \tilde{\phi} G^a_{\mu\nu}. \tag{1.33}$$

Here, $\overline{q}_{2,L}$ is the second generation, left-handed quark doublet, $\sigma^{\mu\nu} = i[\gamma_\mu, \gamma_\nu]/2$ with the Dirac matrices γ_μ , $T^a c$ are the generators of the SU(3), $\tilde{\phi}$ is the adjoint Higgs doublet and $G^a_{\mu\nu}$ is the field strength tensor of the strong interaction. This operator $\hat{O}_{cG}$ may be uniquely bounded with the cH process. This is due to two main factors, including the unique chiral structure of the operator, which mixes left and right-handed spinors, otherwise only found in the Yukawa and quark-Higgs boson interaction terms of the SM.

To better understand this, it is worth considering other processes such as inclusive Higgs boson production, which have been successfully leveraged to set strong contraints on the top quark CMD operator $\hat{O}_{tG}$ [**askNordin**]. Typically, the strategy that is used to probe even small wilson coefficients e.g. C_tG is to exploit interference of the relevant (small) SMEFT contribution with a larger SM contribution. Though the pure SMEFT contribution itself may be small and

experimentally neglible due to limited analysis sensitivity, the much larger contribution of the SM process it interfers with can result in a non-neglible interference effect with respect to the SM process. However, the chiral structure of the CMD operator influences the effectiveness of this strategy. Since the $\hat{O}_{qG}$ operator effectively flips the chirality of the ingoing and outgoing quarks, a second *chirality flip* must be inserted for the SMEFT contribution to interfere with the SM process. This is visualised in **??**. Such a chirality flip is proportional to the mass m_q of the respective quark. As a result the interference contribution for a much lighter quark is significantly supressed, as also argued for the bottom quark in [19]. Effectively, the processes that prove effective in targeting $\hat{O}_{tG}$ due to the large mass of the top quark are much less sensitive to $\hat{O}_{cG}$. Due to the cH process itself containing the chirality flipping quark-Higgs boson vertex, interference terms between the EFT and SM contributions do not suffer from such an effect. Furthermore, due to the very low expected cross section of the cH process, quadratic contributions from $\hat{O}_{cG}$ may be comparatively large even at small values of C_cG. As a result, the cH process may be an excellent target in constraining $\hat{O}_{cG}$.

1.4.2 Validity of an EFT

In addition to EFT terms needing to satisfy the gauge invariance conditions of the SM, two additional key validity conditions are typically required of an EFT. The first is related to the fact that in an EFT, the particle nature of e.g. new, heavy mediator particles is simplified into the introduction of a new effective vertex. For example, a 2→2 particle resonant scattering via a new heavy mediator particle Ω with a newly introduced coupling constant g_* is simplified via the introduction of a four-point interaction, as visualised in **??**. This corresponds to a a first order approximation of the new particle's mediator as

$$\frac{g_*}{p^2 - m_\Omega} \quad \xrightarrow[m_\Omega^2 \gg p^2]{} \quad -\frac{g_*}{m_\Omega}\left(1 + \frac{p^2}{m_\Omega^2} + \frac{p^4}{m_\Omega^4} + ...\right) \approx -\frac{g_*}{m_\Omega} \tag{1.34}$$

For the EFT description of this simplification to be valid, the energy involved in processes containing the effective vertex introduced by the relevant operator must thus lie well below m_Ω, which represents the previously introduced new physics scale Λ. Practically, this can be achieved by placing an upper limit $\mathrm{M_{cut}}$ on the total energy that is considered in measurements of such processes. The requirement can be expressed as

$$\mathrm{M_{cut}} < \Lambda. \tag{1.35}$$

A good estimator of $\mathrm{M_{cut}}$ is the inviariant mass of the final state particles of a process. In case of the cH process, the invariant mass of the Higgs boson and jet system is a natural choice.

The second condition that must be met is related to the perturbativity of the theory. Concretely, this means that higher dimensional operators should contribute increasingly smaller corrections so that the sum of operator contributions converges. In the case of this work where only d=6 operators are considered, this means ensuring contributions from d=8 operators are sufficiently small. While this cannot be determined with certainty without explicit knowledge of the underlying theory the EFT is estimating, a popular choice is to require that at most $g_* \sim 4\pi$ [20].

These two conditions may be combined into a single, simultaneous requirement. In [20] an

effective lagrangian (ignoring relevant indices for simplicity) of the general form

$$\mathcal{L}_{\text{eff}} = \frac{\Lambda^4}{g_*^2}\mathcal{L}\left(\frac{D_\mu}{\Lambda}, \frac{g_h\phi}{\Lambda}, \frac{g_{\psi_{L,R}}\psi_{L,R}}{\Lambda^{3/2}}, \frac{gF_{\mu\nu}}{\Lambda^2}\right) \tag{1.36}$$

is obtained when a single BSM coupling g_* is introduced. This provides a prescription for the powers of the couplings and Λ that are associated with the SM fields ϕ, ψ and $F_{\mu\nu}$, and the covariant derivate D_μ. Here, g represents the unaltered gauge field couplings of the SM, while $g_{\psi_{L,R}}$ and g_h represent the coupling of SM fermion and the Higgs doublet to the BSM theory. In a single BSM coupling scenario, this simplifies to $g_{\psi_{L,R}} = g_h = g_*$. Applying this prescription to the CMD operator gives

$$\hat{O}_{cG} \longrightarrow \frac{\Lambda^4}{g_\star^2}\left[\left(\frac{g_\star\psi_{L,R}}{\Lambda^{3/2}}\right)\cdot\left(\frac{g_\star\psi_{L,R}}{\Lambda^{3/2}}\right)\cdot\left(\frac{g_\star\phi}{\Lambda}\right)\cdot\left(\frac{g_sG}{\Lambda^2}\right)\right] \tag{1.37}$$

$$= \frac{g_\star g_s}{\Lambda^2}\left(\psi_{L,R}\cdot\psi_{L,R}\cdot\phi\cdot G\right). \tag{1.38}$$

Reading off from Equation 1.38, one can see that the coupling of the CMD operator is given by $g_\star g_s/\Lambda^2$. Comparing to Equation 1.30 thus reveals that the CMD Wilson coefficient is given by $C_{cG} = g_* g_s$. By requiring the first validity condition, the relation

$$\frac{C_{cG}}{\Lambda^2} < \frac{g_* g_s}{\mathrm{M}_{\text{cut}}^2} \tag{1.39}$$

is obtained. Since both C_{cG} and Λ are a priori unknown, we can redefine $\tilde{C}_{cG} = \frac{C_{cG}}{\Lambda^2}$. With this redefinition and by setting $g_* \sim 4\pi$, the expression

$$\frac{\left|\tilde{C}_{cG}\right| M_{\text{cut}}^2}{4\pi g_s} < 1\,. \tag{1.40}$$

can be used to define a plane in $\tilde{C}_{cG}$ and M_{cut} that satisfies the previously discussed conditions.

Chapter 2

The CMS experiment at the LHC

The Compact Muon Solenoid (CMS) detector [**CMSDetector**] is large, general purpose particle detector located at the Large Hadron Collider (LHC)[**LHC**] accelerator in Geneva, Switzerland. Run by the European Oragnisation for Nuclear Research (CERN), the LHC's largest ring spans a circumference of 27km, making it the largest particle accelerator in the world. In their circular trajectory through the beam pipe, collimated bunches of $\sim 10^{11}$ protons are accelerted in both directions of the ring. At each of the four collision points, of which CMS is built around one, the trajectories of these proton bunches are crossed such that highly energetic proton-proton collisions are produced. A detector such as CMS effectively acts as a camera taking very complex snapshot of each collision. During Run 2 of the LHC, approximately 30 protons collide on average per bunch crossing with a centre of mass energy of $\sqrt{s} = 13$ TeV. These collisions produce a plethora of particle, many of which decay to particles of varying multiplicities themselves. As such, these collision produce a complex and varied phenomenology that require a complex machine such at the CMS detector to fully capture. By capturing the information from many millions of collisions, a multitude of different statistical analyses may be performed on the captured data. This includes analyses of the Higgs boson and its properties, such as the Yukawa coupling of the charm quark. To this end, this chapter gives an overview of the CMS detector and its subsystems as well as the techniques used to reconstruct individual proton-proton collisions.

2.1 The CMS detector

The CMS detector is designed to be able to detect a wide range of signatures and is built from a set of complementary sub-detectors. An overview of the detector may be seen in Figure 2.1. By combining data from these sub-detectors, a comprehensive reconstruction of individual proton-proton collisions, commonly referred to as an *event*, may be made. The role and functioning of the individual sub-detectors is covered in this section.

2.1.1 The CMS coordinate system

Due to the cylindrical nature of the CMS detector, using cylindrical coordinates to describe positions within the detector is a natural choice. Thus, the z coordinate describes the position along the beam pipe, r the radius and ϕ the azimuthal angle, where the proton-proton collision point is taken as a the coordinate system's centre. Trajectories of particles with energy E within the detector into the plane perpendicular to z may be described by the rapidity

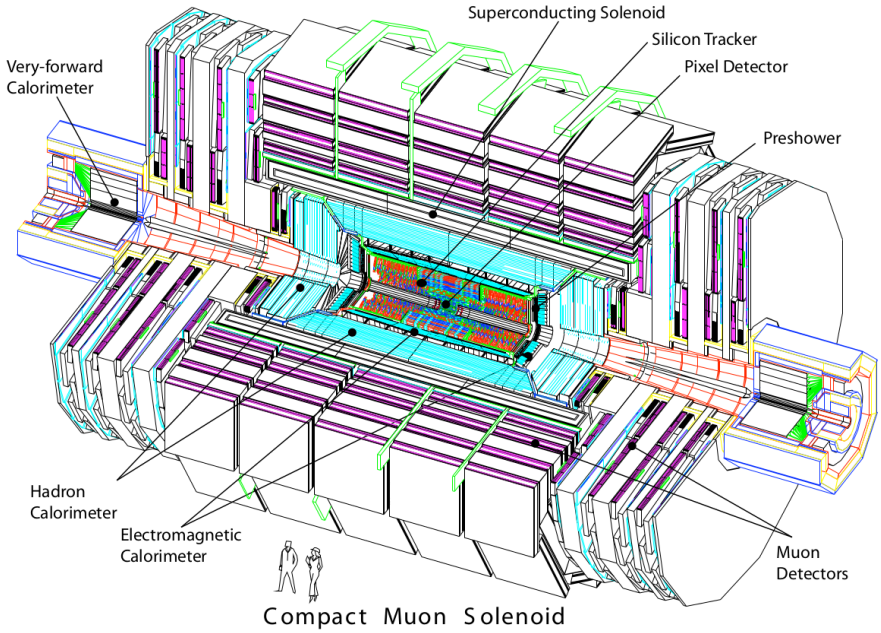

Figure 2.1: An overview of the CMS detector [21].

$$y = \ln \sqrt{\frac{E + p_z c}{E - p_z c}}. \tag{2.1}$$

Small momenta in the z-direction p_z give a rapidity of zero, while the radpitity tends to $\pm\infty$ for large p_z. However, this requires knowledge of E and p_z, which can be difficult to measure. By assuming the particle is ultra-relativistic, as is typically the case at the LHC, it is possible to simply this description and introduce the pseudorapidity

$$\eta = \ln\left(\tan\left(\frac{\theta}{2}\right)\right) \tag{2.2}$$

which is dependent solely on θ, the polar angle. A convenient feature of the (pseudo)rapidity is that differences of (pseudo)rapidity are Lorentz invariant and thus not dependant on the initial longitudinal boost of the proton-proton system, which is a priori not known due to the varying momenta fractions of its constitutents. Together with the particle's transverse (to the beam axis) momentum $\mathrm{p_T}$ and mass m, a particles four-vector may be defined as

$$p = \begin{pmatrix} m \\ p_T \\ \eta \\ \phi \end{pmatrix}. \tag{2.3}$$

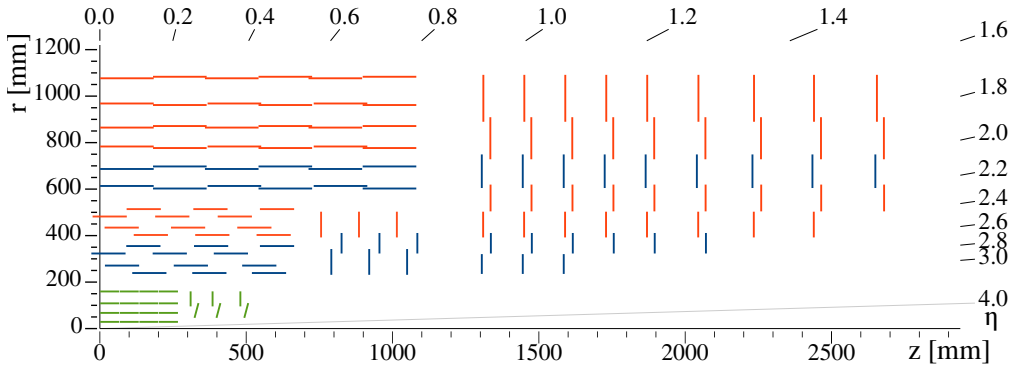

Figure 2.2: An overview of the CMS silicon tracker [22], shown in the r-z plane after its upgrade during Run-2. The pixel detector is denoted in green while the silicon strip detector is denoted in blue and orange.

The CMS detector may be broadly split into two distinct regions inward and outward of the boundary $|\eta| = 1.479$. The inner region or *barrel* consists of concentric layers around the beam pipe. The outer *endcap* region consists of two caps that close off the detector at either end. In this way, the CMS detectors is designed for the best possible hermetic coverage around the collision point.

2.1.2 The silicon tracker

The silicon tracker [22] is the innermost system of the CMS detector, situated closest to the beampipe. It is designed to track the trajectories of charged particles as they emerge from the collision point with minimal energy losses to the particles themselves. This subdetector is split into two main components, the pixel detector and silicon strip detector. A sketch of these components may be seen in Figure 2.3.

The pixel detector is situated right around the beampipe and as of 2017 consists of four circular layers of individual silicon pxiels in the barrel region and three disk layers in the endcap region. These consist of rectangular silicon chips with a size of 100 x 150 μm^2. When a charged particle traverses through the active material of these chips, an electrical signal is induced that is recorded. The small pixel size allows for position measurements with very high resolution, namely $\sim 10\mu$m in the $r\phi$ direction and $\sim 20\mu$m in the z direction [23]. An important feature of the pixel detector its high radiation tolerance due to the close proximity of these modules to the beam pipe.

Following the pixel detector is the silicon strip detector. It is composed of silicon strips of varying sizes, with increases in size at greater distances to the beam pipe due to the reduced overall particle flux they must contend with. In the barrel region, this consists of 10 layers of silicon strips, while in the endcap regions this consists of nine layers. The latter extend the coverage of the detector to $|\eta|$=2.5.

The tracking system provides key information that is essential to the reconstruction of events. As charged particle fly through the CMS detector, their trajectories are curved due to the magnetic field generated by the solenoid magnet (see subsection 2.1.5). By measuring the curvature of these trajectories with this system, the transverse momentum p_T of particles can be constructed.

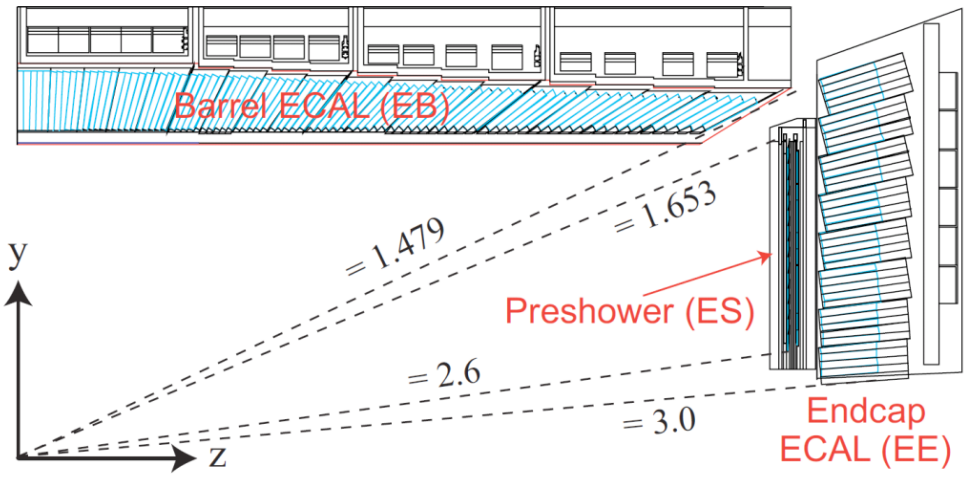

Figure 2.3: An overview of the CMS ECal [25], shown in the r(y)-z plane. The dashed lines denote the coverage of the barrel and endcap ECAL region as well as the preshower detector.

Additionally, the tracker plays a key role in methods used to determine the flavour of a quark that initiates a particle cascade, referred to as a jet (see **??** and **??** for further details). In preparation for the currently ongoing Run-3 of the LHC, the tracking system has since undergone further changes [**Run3Tracker**].

2.1.3 The electromagnetic calorimeter

The second innermost subsystem is the electromagnetic calorimeter (ECAL) [24]. It is designed to measure the energies of electromagnetic showers initiated by photons and electrons. The ECAl is a homogenous calorimeter, consisting of over 75,000 lead tungstate crystals. These crystals scintillate as charged particles pass through them and the produced photons can be collected via photodiodes, producing an electrical signal. This signal may be evaluated to infer the energy that is deposited. Not only do the crystals scintillate but they are also extremely dense and thus are very effective in absorbing the energy of incoming electrons and photons. This allows a very compact thickness of 23cm (22cm) in the barrel (endcap) region, which corresponds to ∼26 (∼25) radiation lengths. An additional component of the ECAl is the preshower detector. This consists of lead absorbers interlaced with scintillating layers and help to distinguish high energy photons from neutral pions. The latter decays into photon pairs which may mimic high energy photons in this part of the detector with an increased likelihood. The increased granularity of the preshower detector helps mitigate this effect. The energy resolution of the ECAl is ∼ 1-4%.

2.1.4 The hadronic calorimeter

Following the ECAl is the hadronic calorimeter (HCAL) [26]. It is designed to measure the presence and energy of hadrons, which typically traverse the ECAL with minor energy losses. It is the most hermetic part of the CMS detector, with a coverage out to $|\eta| = 5.0$, in order to absord almost all collision particles. The only exceptions to this are muons which are particles

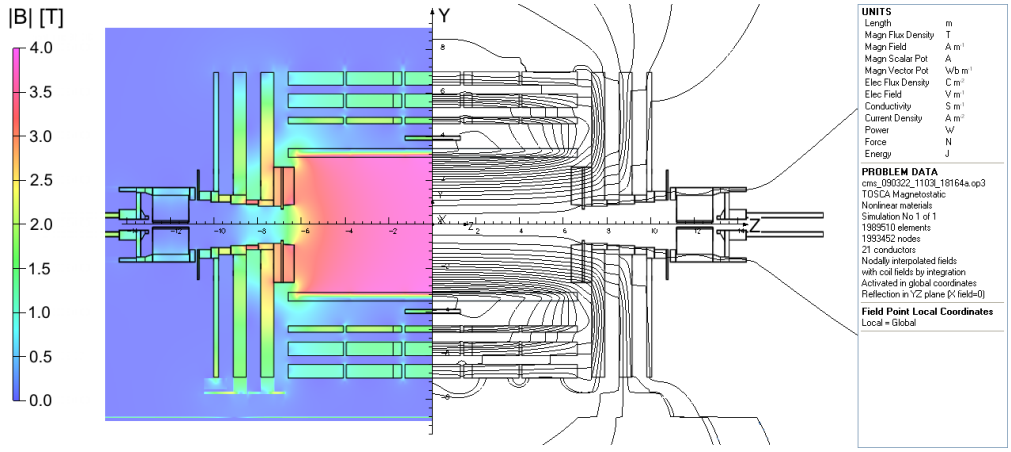

Figure 2.4: An overview of the magnetic flux (left) and magnetic field lines(right) inside the CMS detector, shown in the r-z plane [28].

that minimally deposit their energy and neutrinos, which have an interaction probability that is so low that they cannot be measured with the CMS detector at all.

In contrast to the ECAL, the HCAL is a sampling calorimeter. This means layers of absorber are interleaved with layers of a scintillator. Different materials are used in different parts of the calorimeter, which is split into the barrel ($|\eta| < 1.5$), endcap ($1.5 < |\eta| < 3.0$) and forward ($3.0 < |\eta| < 5.0$) regions. Since the HCAL component inside the magnet system does not sufficiently absorb all hadronic showers, the system also extends past the magnet. Due to the sampling nature of the calorimeter, a lower nuber of respective interaction lengths and larger energy fluctuations in hadronic particle showers, the energy resolution of the HCAL is significantly poorer than the ECAL. It lies in the order of 10-30% and is greatly dependent on the energy and pseudorapidity of the initiating particles.

2.1.5 The superconducting solenoid magnet

A key component of the CMS detector is the superconducting solenoid magnet [27]. It is responsible for maintaining a strong 3.8 T magnetic field that homogenously permeats the barrel of the detector. A measurement of the field strength can be seen in Figure 2.4. With its toroidal shape, the field is orientated along the z-axis and covers the 12.9m barrel region of the detector, curving the the trajectories of charged particles emerging from the interaction point in the ϕ-direction. This allows for a measurement of the particles transverse momentum p_T, which together with the ϕ and η directions fully characterise the particle's momentum vector. The magnet itself is composed of of superconducting noibium-titanum coils that must be cooled to a temperature of 4.65K, at which these are superconducting. The magnet is encased by a 12,000t steel yoke that captures the magentic field that is produced outside of the solenoid.

2.1.6 The muon chambers

2.1.7 The triggering system

2.2 Event reconstruction with the CMS detector

Chapter 3

Search for the cH(ZZ$\rightarrow 4\mu$) process

Chapter 4

An EFT interpretation of the cH(ZZ→4μ) process

Conclusion

Bibliography

[1] S. Navas et al. "Review of Particle Physics". In: *Phys. Rev. D* 110 (3 Aug. 2024), p. 030001. DOI: 10.1103/PhysRevD.110.030001. URL: https://link.aps.org/doi/10.1103/PhysRevD.110.030001.

[2] P.W. Higgs. "Broken Symmetries and the Masses of Gauge Bosons". In: *Phys. Rev. Lett.* 13 (16 Oct. 1964), pp. 508–509. DOI: 10.1103/PhysRevLett.13.508. URL: https://link.aps.org/doi/10.1103/PhysRevLett.13.508.

[3] F. Englert and R. Brout. "Broken Symmetry and the Mass of Gauge Vector Mesons". In: *Phys. Rev. Lett.* 13 (9 Aug. 1964), pp. 321–323. DOI: 10.1103/PhysRevLett.13.321. URL: https://link.aps.org/doi/10.1103/PhysRevLett.13.321.

[4] CMS Collaboration. "Observation of a new boson at a mass of 125 GeV with the CMS experiment at the LHC". In: *Physics Letters B* 716 (1 2012), pp. 30–61. DOI: 10.1016/j.physletb.2012.08.021.. URL: https://www.sciencedirect.com/science/article/pii/S0370269312008581.

[5] G. Aad et al. "Observation of a new particle in the search for the Standard Model Higgs boson with the ATLAS detector at the LHC". In: *Physics Letters B* 716.1 (2012), pp. 1–29. ISSN: 0370-2693. DOI: 10.1016/j.physletb.2012.08.020. URL: https://www.sciencedirect.com/science/article/pii/S037026931200857X.

[6] CMS Collaboration. "A portrait of the Higgs boson by the CMS experiment ten years after the discovery". en. In: *Nature* 607.7917 (July 2022), pp. 60–68. DOI: 10.1038/s41586-022-04892-x. URL: http://dx.doi.org/10.1038/s41586-022-04892-x.

[7] Nina M. Coyle, Carlos E. M. Wagner, and Viska Wei. "Bounding the charm Yukawa coupling". In: *Phys. Rev. D* 100 (7 Oct. 2019), p. 073013. DOI: 10.1103/PhysRevD.100.073013. URL: https://link.aps.org/doi/10.1103/PhysRevD.100.073013.

[8] Michael Edward Peskin and Daniel V. Schroeder. *An Introduction to Quantum Field Theory*. Reading, USA: Addison-Wesley (1995) 842 p. Westview Press, 1995.

[9] R. Wolf. *The Higgs Boson Discovery at the Large Hadron Collider*. Springer, 2015. ISBN: 978-3-319-18512-5, 978-3-319-18511-8. DOI: 10.1007/978-3-319-18512-5.

[10] G. Arnison et al. "Experimental observation of isolated large transverse energy electrons with associated missing energy at s=540 GeV". In: *Physics Letters B* 122.1 (1983), pp. 103–116. ISSN: 0370-2693. DOI: 10.1016/0370-2693(83)91177-2. URL: https://www.sciencedirect.com/science/article/pii/0370269383911772.

[11] J. Goldstone, A. Salam, and S. Weinberg. "Broken Symmetries". In: *Phys. Rev.* 127 (3 Aug. 1962), pp. 965–970. DOI: 10.1103/PhysRev.127.965. URL: https://link.aps.org/doi/10.1103/PhysRev.127.965.

[12] CMS Collaboration. *Simultaneous probe of the charm and bottom quark Yukawa couplings using ttH events*. 2025. DOI: 10.48550/arXiv.2509.22535. arXiv: 2509.22535 [hep-ex]. URL: https://arxiv.org/abs/2509.22535.

[13] CMS Collaboration. *Search for a Higgs boson produced in association with a charm quark and decaying to a W boson pair in proton-proton collisions at $\sqrt{s}$ = 13 TeV*. 2025. arXiv: 2508.14988 [hep-ex]. URL: https://arxiv.org/abs/2508.14988.

[14] CMS Collaboration. *Search for the associated production of a Higgs boson with a charm quark in the diphoton decay channel in pp collisions at $\sqrt{s}$ = 13 TeV*. 2025. arXiv: 2503.08797 [hep-ex]. URL: https://arxiv.org/abs/2503.08797.

[15] Nuoyu Dong et al. "Probing charm Yukawa coupling through *ch* associated production at the hadron colliders". In: *Phys. Rev. D* 111 (5 Mar. 2025), p. 053003. DOI: 10.1103/PhysRevD.111.053003. URL: https://link.aps.org/doi/10.1103/PhysRevD.111.053003.

[16] C T Potter et al. *Handbook of LHC Higgs Cross Sections: 3. Higgs Properties: Report of the LHC Higgs Cross Section Working Group*. en. 2013. DOI: 10.5170/CERN-2013-004. URL: http://cds.cern.ch/record/1559921.

[17] J. A. Aguilar-Saavedra, J. M. Cano, and J. M. No. "More light on Higgs flavor at the LHC: Higgs boson couplings to light quarks through $h + \gamma$ production". In: *Phys. Rev. D* 103 (9 May 2021), p. 095023. DOI: 10.1103/PhysRevD.103.095023. URL: https://link.aps.org/doi/10.1103/PhysRevD.103.095023.

[18] The CMS Collaboration. "Combined measurements of Higgs boson couplings in proton–proton collisions at $\sqrt{s} = 13\,\text{TeV}$". In: *The European Physical Journal C* 79.5 (May 2019). ISSN: 1434-6052. DOI: 10.1140/epjc/s10052-019-6909-y. URL: http://dx.doi.org/10.1140/epjc/s10052-019-6909-y.

[19] Joseph Bramante et al. "Boosted Higgs bosons from chromomagnetic *b*'s: $b\bar{b}h$ at high luminosity". In: *Phys. Rev. D* 93 (5 Mar. 2016), p. 053001. DOI: 10.1103/PhysRevD.93.053001. URL: https://link.aps.org/doi/10.1103/PhysRevD.93.053001.

[20] J. Elias-Miró et al. "Higgs windows to new physics through d=6 operators: constraints and one-loop anomalous dimensions". In: *Journal of High Energy Physics* 2013.11 (Nov. 2013). ISSN: 1029-8479. DOI: 10.1007/jhep11(2013)066. URL: http://dx.doi.org/10.1007/JHEP11(2013)066.

[21] The CMS Collaboration. *CMS Physics : Technical Design Report Volume 1: Detector Performance and Software*. Technical design report. CMS. Geneva: CERN, 2006. URL: https://cds.cern.ch/record/922757.

[22] *CMS Tracker Detector Performance Public Results*. Last accessed 24.11.25. URL: https://twiki.cern.ch/twiki/bin/view/CMSPublic/DPGResultsTRK.

[23] The CMS Collaboration. "Description and performance of track and primary-vertex reconstruction with the CMS tracker". In: *Journal of Instrumentation* 9.10 (Oct. 2014), P10009–P10009. ISSN: 1748-0221. DOI: 10.1088/1748-0221/9/10/p10009. URL: http://dx.doi.org/10.1088/1748-0221/9/10/P10009.

[24] CMS Collaboration. *The CMS electromagnetic calorimeter project: Technical Design Report*. Tech. rep. Geneva, 1997. URL: https://cds.cern.ch/record/349375.

[25] CMS Collaboration. *The CMS ECAL performance with examples*. Tech. rep. Geneva: CERN, 2014. DOI: 10.1088/1748-0221/9/02/C02008. URL: https://cds.cern.ch/record/1632384.

[26] CMS Collaboration. *The CMS hadron calorimeter project: Technical Design Report*. Tech. rep. Geneva, 1997. URL: https://cds.cern.ch/record/357153.

[27] CMS Collaboration. *The CMS magnet project: Technical Design Report*. Tech. rep. Geneva, 1997. URL: https://cds.cern.ch/record/331056.

[28] CMS Collaboration. "Precise mapping of the magnetic field in the CMS barrel yoke using cosmic rays". In: *Journal of Instrumentation* 5.03 (Mar. 2010), T03021–T03021. ISSN: 1748-0221. DOI: 10.1088/1748-0221/5/03/t03021. URL: http://dx.doi.org/10.1088/1748-0221/5/03/T03021.